

## Electronic structure and magneto-optics of self-assembled quantum dots

Arkadiusz Wojs

*Institute for Microstructural Sciences, National Research Council of Canada, Ottawa, Canada K1A 0R6  
and Institute of Physics, Technical University of Wrocław, Wybrzeże Wyspiańskiego 27, 50-370 Wrocław, Poland*

Paweł Hawrylak and Simon Fafard

*Institute for Microstructural Sciences, National Research Council of Canada, Ottawa, Canada K1A 0R6*

Lucjan Jacak

*Institute of Physics, Technical University of Wrocław, Wybrzeże Wyspiańskiego 27, 50-370 Wrocław, Poland  
(Received 8 November 1995)*

The electronic structure of lens-shaped self-assembled quantum dots is studied as a function of the dot size, the confining potential, and the magnetic field. The parabolic confining potential and its corresponding energy spectrum are shown to be an excellent approximation. The magnetoexciton spectrum is calculated and compared with recent experiments. [S0163-1829(96)02932-3]

### I. INTRODUCTION

Recent progress in the growth techniques produced high-quality quasi-two-dimensional self-assembled dots (SAD).<sup>1</sup> Due to efficient recombination processes even at room temperature,<sup>2-4</sup> these systems show promise as lasers and hole burning based optical memories. A recent demonstration of charging of SAD with free carriers<sup>5</sup> without introducing unnecessary large potential fluctuations, inherent in modulation doped quantum dots, shows possibilities of electronic applications.

The shape of the dot depends on growth conditions. Dots in the shape of pyramids,<sup>6</sup> cones,<sup>7</sup> disks,<sup>8-10</sup> and lenses<sup>1,2,4,5</sup> have been studied, although the actual determination of the shape is not definite. We concentrate here on lens-shaped SAD.<sup>1,5,3,4</sup> Depending on the growth parameters, different sizes of lens-shaped SAD have been reported but there is at present no clear correlation between the electronic structure and the shape and the size of SAD. We use the effective mass approximation to study the dependence of energy levels of lens-shaped SAD on size, depth of confining potential, and the magnetic field. In such SAD both electrons and holes are confined and magneto-optics should be a useful tool in relating structural parameters to the photoluminescence and absorption spectrum.<sup>9,11</sup> In order to do so, a calculation of magnetoexciton energies and oscillator strengths is necessary. We present here such calculations and relate the electron and hole energy levels to the magneto-optical properties of the SAD.

### II. ELECTRONIC STATES

A schematic picture of a lens-shaped SAD formed on a wetting layer (WL) of thickness  $t_w$ , and modeled as a part of a sphere with fixed height  $h$  and radius at the base  $s$  is shown in Fig. 1. Most of the reported samples with different sizes are characterized by a constant ratio of the height  $h$  to the radius  $s$ .<sup>12,13</sup> The bottom of the conduction band (CB) of the WL and SAD material (e.g.,  $\text{In}_{0.5}\text{Ga}_{0.5}\text{As}$ ) is below the bot-

tom of the CB of the surrounding material (e.g., GaAs).<sup>2,4</sup> The carriers, confined to a narrow WL quantum well, are further localized in the area of the dot due to the effectively increased thickness of the layer. The resulting net confining potential  $V(r, z)$  has been shown in the inset of Fig. 1.

The parameters of WL and SAD material enter through the effective Rydberg  $\mathcal{R}^* = m_e e^4 / 2 \epsilon^2 \hbar^2 \equiv 1$  and the effective Bohr radius  $a_B^* = \epsilon \hbar^2 / m_e e^2 \equiv 1$ , with  $m_e$  and  $\epsilon$  being the effective mass of an electron and the dielectric constant, respectively. These effective parameters include all effects due to strain, discontinuities in the effective mass, dielectric constants, etc.

In the effective mass approximation the Schrödinger equation for the electrons in cylindrical coordinates reads

$$\left[ -\frac{1}{r^2} \left( r \frac{\partial}{\partial r} r \frac{\partial}{\partial r} + \frac{\partial^2}{\partial \theta^2} \right) - \frac{\partial^2}{\partial z^2} + V_e(r, z) \right] \psi(r, \theta, z) = E \psi(r, \theta, z), \quad (1)$$

with  $V_e = 0$  inside the WL and SAD, and  $V_e = V_0$  inside the barrier ( $V_0 = \Delta V_{\text{CB}}$  is the difference in conduction-band energies in the two materials including the effects of strain).

We have used two approaches to the solution of the three-dimensional (3D) Schrödinger equation: (a) full 3D numerical diagonalization, where in order to construct the suitable discrete basis the system was embedded in the large infinite-wall disk, and (b) adiabatic approximation. Since the full numerical diagonalization justified the use of the adiabatic approximation, we shall only discuss the latter approach as by far more physically intuitive.

In the adiabatic approximation, we take advantage of the fact that the electron's wave function is strongly confined to the lowest subband of the narrow quantum well of the WL. We therefore write the wave function as  $\psi(r, \theta, z) = (1/\sqrt{2\pi}) e^{im\theta} g_r(z) f_m(r)$ , where  $g_r(z)$  is a slowly varying function of  $r$ . Wave functions  $g$  and  $f_m$  satisfy a set of equations for each angular momentum channel  $m$ :

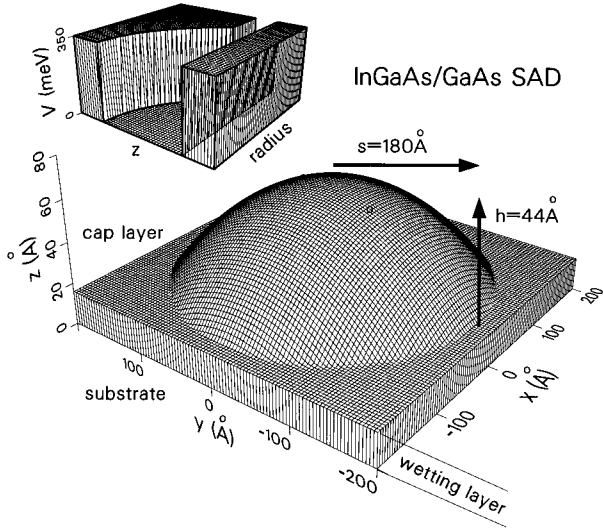


FIG. 1. A schematic picture of the  $\text{In}_x\text{Ga}_{1-x}\text{As}/\text{GaAs}$  self-assembled dot modeled as a part of the sphere on the narrow wetting layer. Inset: effective lateral potential confining electrons due to varying thickness of  $\text{In}_x\text{Ga}_{1-x}\text{As}$  layer.

$$\left[ -\frac{\partial^2}{\partial z^2} + V_e(r, z) \right] g_r(z) = E_0(r) g_r(z), \quad (2)$$

$$\left[ -\frac{1}{r^2} \left( r \frac{\partial}{\partial r} r \frac{\partial}{\partial r} - m^2 \right) + E_0(r) \right] f_m(r) = E f_m(r). \quad (3)$$

We first find the energy  $E_0(r)$  corresponding to the motion in the  $z$  direction for a given thickness of the structure at the distance  $r$  from the center of the dot (this is the effective lateral potential  $V$  shown in the inset in Fig. 1). Next, the radial motion in the potential  $E_0(r)$  is solved exactly for each angular momentum channel. This is accomplished by approximating  $E_0(r)$  by the  $n$ -step piecewise potential:  $V(r) = v_i$  if  $s_i \leq r \leq s_{i+1}$ , where  $0 \leq i \leq n$ ,  $s_0 = 0$ ,  $s_{n+1} = \infty$ ,  $s_i < s_{i+1}$ ,  $v_i < v_{i+1}$ . The wave function corresponding to energy  $E$  and angular momentum  $m$  can be written in a compact form:

$$f_m(r) = A_i F(k_i r) + B_i G(k_i r) \quad \text{if } s_i \leq r \leq s_{i+1}, \quad (4)$$

where  $k_i^2 = |E - v_i|$ , and  $(F, G)$  are the appropriate pair of Bessel functions:  $(J_m, Y_m)$  if  $E > v_i$ , and  $(K_m, I_m)$  if  $E < v_i$ . The wave functions must be continuous and smooth at each interface:

$$A_{i-1} F_i^L + B_{i-1} G_i^L = A_i F_i^R + B_i G_i^R, \quad (5)$$

$$A_{i-1} \nabla F_i^L + B_{i-1} \nabla G_i^L = A_i \nabla F_i^R + B_i \nabla G_i^R, \quad (6)$$

where we introduced the notation  $\mathcal{F}_i^L \equiv \mathcal{F}(k_{i-1} s_i)$ ,  $\mathcal{F}_i^R \equiv \mathcal{F}(k_i s_i)$ ,  $\nabla \mathcal{F}_i^L \equiv k_{i-1} \mathcal{F}'(k_{i-1} s_i)$ ,  $\nabla \mathcal{F}_i^R \equiv k_i \mathcal{F}'(k_i s_i)$ ,  $\mathcal{F} = F, G$ . The relation between coefficients  $(A, B)$  can be written in terms of transfer matrices  $\hat{T}_j$ :

$$\begin{bmatrix} A_j \\ B_j \end{bmatrix} = \hat{T}_j \begin{bmatrix} A_{j-1} \\ B_{j-1} \end{bmatrix}. \quad (7)$$

Following from Eqs. (5) and (6):

$$\hat{T}_j = \begin{pmatrix} F_j^R & G_j^R \\ \nabla F_j^R & \nabla G_j^R \end{pmatrix}^{-1} \begin{pmatrix} F_j^L & G_j^L \\ \nabla F_j^L & \nabla G_j^L \end{pmatrix}. \quad (8)$$

Solving Eqs. (5) and (6) is equivalent to finding the total transfer matrix  $\hat{T}$ , defined as

$$\begin{bmatrix} A_n \\ B_n \end{bmatrix} = \left( \prod_{i=1}^n \hat{T}_i \right) \begin{bmatrix} A_0 \\ B_0 \end{bmatrix} \equiv \hat{T} \begin{bmatrix} A_0 \\ B_0 \end{bmatrix}. \quad (9)$$

As the wave functions must be finite at the origin we have  $B_0 = 0$ .

The bound-state energies  $E_b$  are obtained by requiring the wave function to decay for large radii. The additional boundary condition,  $B_n = 0$ , translates into vanishing of the corresponding element of the total transfer matrix:  $T_{21}(E_b) = 0$  for a discrete set of energies  $E_b$ .

For energy  $E$  in the WL continuum electrons are scattered by the quantum dot potential. The scattering modifies the density of states (DOS). The phase shift  $\eta_m(E)$  corresponding to energy  $E$  and angular momentum  $m$  can be expressed by the transfer matrix as

$$\eta_m = \arg(T_{11} - iT_{21}) \quad (10)$$

and the change in DOS is

$$\delta D(E) = \sum_m \frac{1}{\pi} \frac{d\eta_m}{dE} \equiv \sum_m \delta D_m(E). \quad (11)$$

Sharp maxima in DOS correspond to resonant scattering states, through which the bound states of the dot can be efficiently populated in, e.g., high-intensity optical experiments.

In Fig. 2 we show the energy spectrum of the  $\text{In}_{0.5}\text{Ga}_{0.5}\text{As}/\text{GaAs}$  SAD (Ref. 4) of dimensions  $s = 180 \text{ \AA}$ ,  $h = 44 \text{ \AA}$ ,  $t_w = 16 \text{ \AA}$ . The effects of strain are approximated by calculating a uniform hydrostatic-pressure shift and a uniaxial stress-induced valence-band (VB) splitting. Assuming a conduction-band offset of 67% the resulting electron confining potential is  $V_0 = 350 \text{ meV}$ , the effective mass of strained  $\text{In}_{0.5}\text{Ga}_{0.5}\text{As}$   $m_e = 0.067$ , and the dielectric constant  $\epsilon = 12.5$ . In the inset we show changes in DOS  $\delta D_m(E)$  in the range of energy corresponding to the WL continuum. For clarity only a few curves giving the strongest resonances have been plotted. These are the ones corresponding to  $m = 1, 3, 6, 7$  (the state with  $m = 5$  is very weakly bound).

Energies of discrete bound states and resonances form the spectrum consisting of almost degenerate and almost equally spaced shells, very well approximated by the cutoff spectrum of the parabolic lateral potential with the intershell spacing of  $\omega_{e,0} = 30 \text{ meV}$ . The number of shells is 5 and the total number of confined states (including  $\pm m$  and spin degeneracy) is 30.

The average size of the dot depends on the growth conditions. The height of the potential barrier  $V_0$  in  $\text{In}_x\text{Ga}_{1-x}\text{As}/\text{GaAs}$  samples varies with In concentration. Below we show the dependence of the energy spectra on these parameters, i.e., the number of confined states, and the average intershell spacing  $\omega_{e,0}$ . The results are presented in Fig. 3, where the energy is measured from the bottom of the

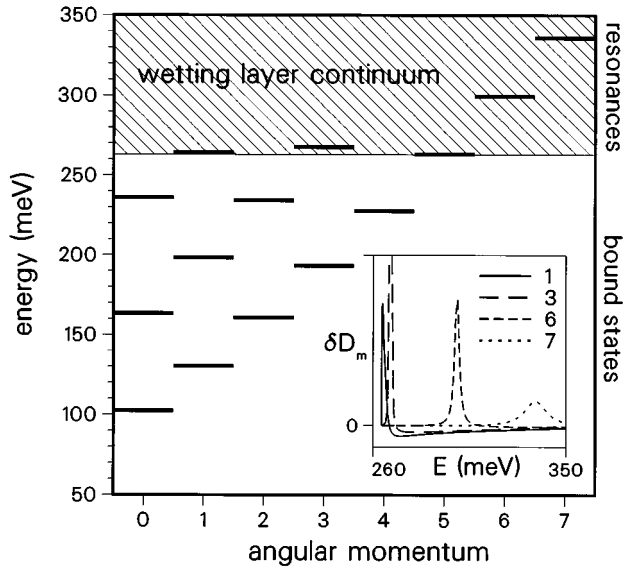


FIG. 2. The energy spectrum of bound states and wetting-layer resonances in the  $\text{In}_x\text{Ga}_{1-x}\text{As}/\text{GaAs}$  dot with radius  $s=180 \text{ \AA}$ , height  $h=44 \text{ \AA}$ , and depth of the confining potential  $V_0=350 \text{ meV}$ . The levels are degenerated due to spin and  $\pm m$  symmetries. Average intershell spacing is  $\omega_{e,0}=30 \text{ meV}$ . Inset: Change in the density of states in the wetting-layer continuum due to scattering potential of the dot (plotted only for a few  $m$  channels with strong resonances).

three-dimensional continuum in the barriers.

The top frame shows the dependence of the spectrum on the size, given by the radius of the dot  $s$ , with a fixed ratio  $h/s=0.24$  and  $V_0=350 \text{ meV}$ . Starting with a single weakly bound  $s$  orbital for  $s < 80 \text{ \AA}$  one can follow the consecutive shells coming down from the WL continuum as the size is increased. The intershell spacing decreases with increasing size and hence the almost ideally paraboliclike spectrum obtained for smaller values of  $s$  evolves into a more complicated structure of levels (the spread of higher shells comparable to intershell separation) for larger dots.

The bottom frame presents the dependence of the spectrum on the potential depth  $V_0$  at fixed size  $s=180 \text{ \AA}$  and  $h=44 \text{ \AA}$ . Analogously to the upper graph we observe a growing number of bound states with increasing  $V_0$ . However, the intershell separation  $\omega_{e,0}$  grows now with increasing  $V_0$ , and therefore also with increasing number of bound states. For the size of the dot chosen for this graph (corresponding to the work of Refs. 2 and 4), the distinct well-separated shells are obtained in the full range of  $V_0$ .

Combining the dependences shown in Fig. 3 one can, at least in principle, design the SAD systems with a desired number of confined states separated by a characteristic intershell excitation energy.

The other useful information following from Fig. 3 is the ability to relate the experimentally measured distribution of the SAD sizes with the inhomogeneously broadened DOS of a sample consisting of many dots. Following the work by Raymond *et al.* we took the Gaussian distribution of sizes with average radius  $\langle s \rangle = 180 \text{ \AA}$  and a standard deviation  $\sigma_s = 10 \text{ \AA}$ . The inhomogeneously broadened DOS is shown in Fig. 5. An important conclusion following from Fig. 5 is

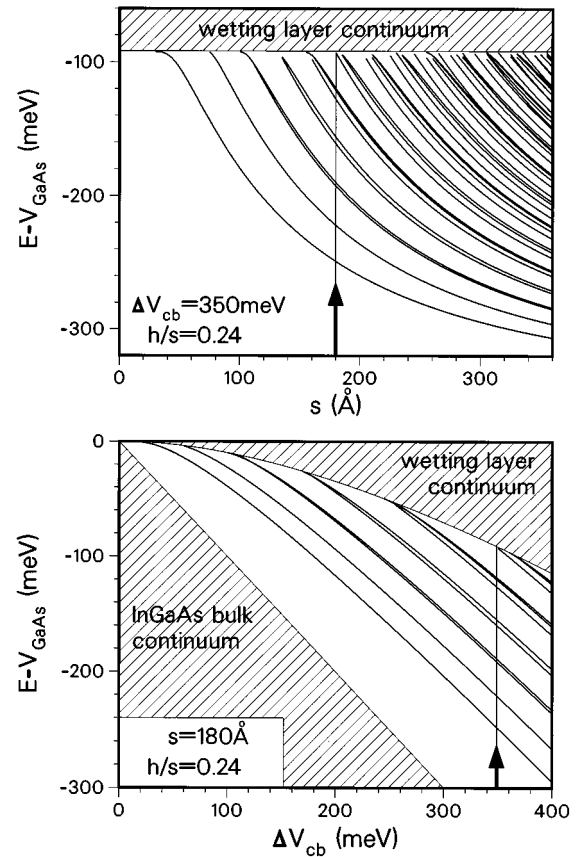


FIG. 3. Dependences of the electronic energy spectrum of the dot on size (top frame) and on the depth of confining potential  $V_0$  (bottom frame). Vertical arrows indicate the spectrum shown in Fig. 2.

that the uniformity of SAD in this sample is sufficient for the sample to retain the spectral 0D density of states of an individual dot.

### III. MAGNETOEXCITONS

We have shown above that the electron energy spectrum in SAD can be described quite well by a cutoff parabolic potential. For strained  $\text{In}_x\text{Ga}_{1-x}\text{As}$  one expects the mixing between light and heavy holes to be small and we therefore approximate the hole energy levels in the same way as for an electron but with a different effective mass and depth of confining potential. Five confined heavy-hole shells have been found, separated by  $\omega_{h,0} = 15 \text{ meV}$ .

For a magnetic field  $B$  along the  $z$  direction and for a parabolic confining potential an electron  $H_e$ , and a hole  $H_h$ , Hamiltonians can be diagonalized exactly. The resulting single-particle energy spectrum is a Fock-Darwin (FD) spectrum  $E_{mn}$  of two independent harmonic oscillators.<sup>15,16</sup> It has been verified (through numerical calculations analogous to those described for  $B=0$ ) that the  $B$  evolution of the energy spectrum for the actual confining potential  $V(r,z)$  is virtually identical to the lowest part of the FD spectrum. The calculation of magnetoexcitons in quantum dots with the FD spectrum has been described in detail in Ref. 14. Here we only

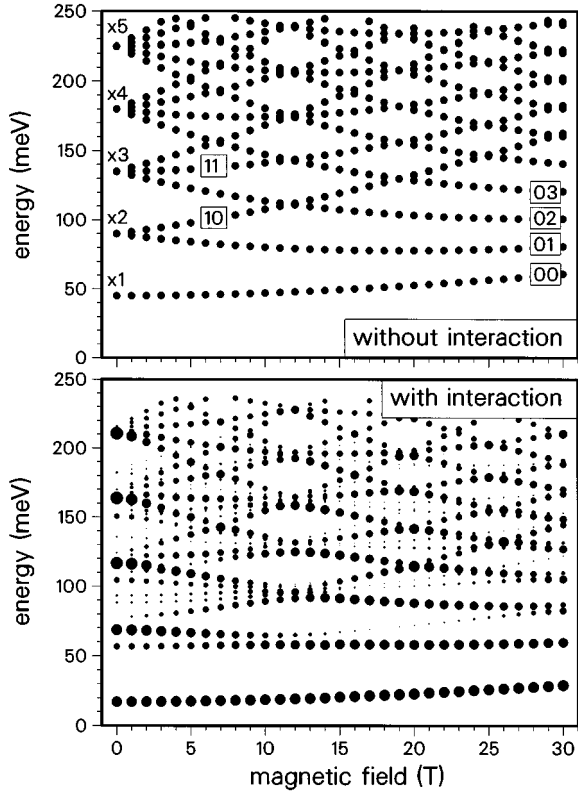


FIG. 4. Evolution of absorption spectrum of a SAD magnetoexciton with the magnetic field (all parameters as in Fig. 2). Areas of dots are proportional to intensities of transitions. Upper and lower frames present graphs for noninteracting and interacting systems, respectively. In the upper frame the degeneracies of overlapping peaks at  $B=0$  have been indicated.

present results of a calculation for the sample studied in Ref. 4.

In Fig. 4 we present the evolution of the absorption spectrum with the increasing magnetic field  $B$ , calculated for the parameters as in Fig. 2. The top frame corresponds to a noninteracting electron-hole pair, and the bottom frame to the interacting magnetoexciton. The areas of black dots are proportional to the intensities of discrete peaks, energies of which (measured from the VB-CB gap) are given on the vertical axis.

For the noninteracting electron-hole pair all peaks are of equal strength and their evolution in  $B$  repeats the FD pattern of each particle. The FD orbitals  $|nm\rangle$  on which the pair is created have been indicated for a few peaks. This picture illustrates the destruction and restoration of the dynamical symmetries of the FD spectrum by the magnetic field. As for certain values of  $B$  (0, 12, 19, 25 T) the levels cross, intensities of neighboring peaks add up around these values of  $B$ , and, e.g., for  $B=0$  the overall intensity rises linearly in energy.

The Coulomb interaction mixes many electron-hole states and leads to a richer energy spectrum, shown in the bottom frame of Fig. 4. Nevertheless, the magnetoexciton spectrum resembles quite well the FD spectrum of the noninteracting electron-hole pair, in particular, the restoration of symmetries and the reappearance of gaps in the spectrum around 13

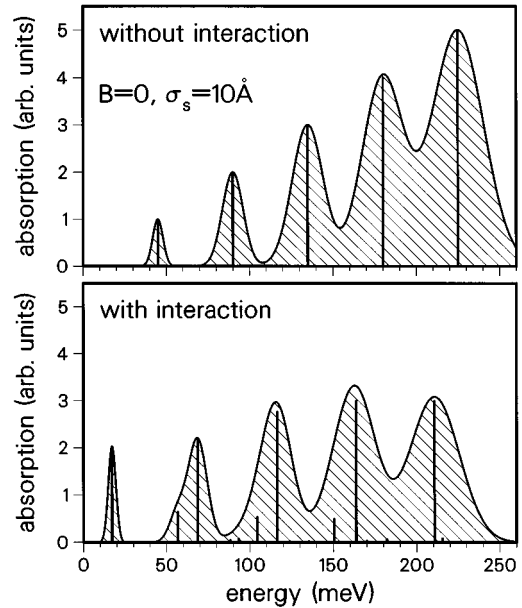


FIG. 5. Absorption spectra of noninteracting (top frame) and interacting (bottom frame) exciton in zero magnetic field, including inhomogeneous broadening of peaks due to the distribution of dot sizes ( $\langle s \rangle = 180 \text{ \AA}$ ,  $\sigma_s = 10 \text{ \AA}$ ). Full bars correspond to discrete peaks obtained for average size.

T. This is because in such small quantum dots the characteristic confinement energy  $\omega_{e,0} + \omega_{h,0}$  ( $\sim 45 \text{ meV}$ ) exceeds the characteristic Coulomb energy ( $\sim 25 \text{ meV}$ , slightly  $B$  dependent). The main effect of including the interaction on the eigenenergies is therefore the parallel redshift of the entire spectrum.

In Fig. 5 the zero-field interacting and noninteracting absorption spectra have been shown, including the inhomogeneous broadening of peaks due to the distribution of dot sizes in the sample. In both frames smearing of the peaks does not exceed  $\omega_{e,0} + \omega_{h,0}$  and five strong maxima originating from five bound shells persist. The modification of the structure of peaks due to the Coulomb interaction consists mainly in moving the intensity of absorption towards lower energies. Consequently, instead of intensity of the peaks linearly increasing in energy due to increasing degeneracy of shells, as is the case of the noninteracting system, high-energy peaks are significantly reduced and the lowest (ground-state) peak is enhanced. For high excitation power all five excited states have been observed by Raymond *et al.*<sup>4</sup> We find the calculated separation between the peaks in good agreement with their experiment.

#### IV. CONCLUSIONS

We have studied the dependence of lens-shaped self-assembled quantum dots on the dot size, the height of the confining potential, and the magnetic field. This should help in designing future structures with required physical properties. The energy structure resembles very well the Fock-Darwin levels of a quantum dot with parabolic confinement. The size dependence of the energy levels shows that the uniformity of currently grown structures is sufficient to over-

come the broadening due to size distribution and the density of states of macroscopic samples is that of an inhomogeneously broadened single quantum dot. The calculated magnetoexciton spectrum shows interesting magnetic field dependence due to the restoration of dynamical symmetries of electronic states by the magnetic field. The zero-magnetic-

field results compare well with recent experiments by Raymond *et al.*

#### ACKNOWLEDGMENTS

This work was supported by NATO HTECH Grant No. 930746 and by the Institute for Microstructural Sciences, NRC Canada.

- 
- <sup>1</sup>P. M. Petroff and S. P. Denbaars, *Superlatt. Microstruct.* **15**, 15 (1994).
- <sup>2</sup>S. Fafard, R. Leon, D. Leonard, J. L. Merz, and P. M. Petroff, *Phys. Rev. B* **52**, 5752 (1995).
- <sup>3</sup>S. Fafard, D. Leonard, J. L. Merz, and P. M. Petroff, *Appl. Phys. Lett.* **65**, 1388 (1994).
- <sup>4</sup>S. Raymond, S. Fafard, P. J. Poole, A. Wojs, P. Hawrylak, S. Charbonneau, D. Leonard, R. Leon, P. M. Petroff, and J. L. Merz, *Phys. Rev. B* (to be published).
- <sup>5</sup>H. Drexel, D. Leonard, W. Hansen, J. P. Kotthaus, and P. M. Petroff, *Phys. Rev. Lett.* **73**, 2252 (1994).
- <sup>6</sup>M. Grundmann, N. N. Ledentsov, R. Heitz, L. Eckey, J. Christen, J. Böhrer, D. Bimberg, S. S. Ruvimov, P. Werner, U. Richter, J. Heydenreich, V. M. Ustinov, A. Y. Egorov, A. E. Zhukov, P. S. Kopev, and Z. I. Alferov, *Phys. Status Solidi B* **188**, 249 (1995).
- <sup>7</sup>J. Y. Marzin and G. Bastard, *Solid State Commun.* **92**, 437 (1994).
- <sup>8</sup>R. Notzel *et al.*, *Appl. Phys. Lett.* **66**, 2525 (1995).
- <sup>9</sup>H. Weman, H. Kamada, M. Potemski, J. Temmyo, R. Notzel, and T. Tamamura, in *Proceedings of Seventh International Conference on Modulated Semiconductor Structures, Madrid, 1995* [Solid State Electron. (to be published)].
- <sup>10</sup>F. M. Peeters and A. Schweigert, *Phys. Rev. B* **53**, 1460 (1996).
- <sup>11</sup>P. D. Wang, J. L. Merz, S. Fafard, R. Leon, D. Leonard, G. Medeiros-Ribeiro, M. Oestreich, P. M. Petroff, K. Uchida, N. Miura, H. Ariyama, and H. Sakaki, *Phys. Rev. B* **53**, 16 458 (1996).
- <sup>12</sup>R. Leon, S. Fafard, D. Leonard, J. L. Merz, and P. M. Petroff, *Appl. Phys. Lett.* **67**, 521 (1995).
- <sup>13</sup>D. Leonard, K. Pond, and P. M. Petroff, *Phys. Rev. B* **50**, 11 687 (1994).
- <sup>14</sup>A. Wojs and P. Hawrylak, *Phys. Rev. B* **51**, 10 880 (1995).
- <sup>15</sup>P. A. Maksym, *Physica B* **184**, 385 (1993); P. A. Maksym and Tapash Chakraborty, *Phys. Rev. Lett.* **65**, 108 (1990); *Phys. Rev. B* **45**, 1947 (1992).
- <sup>16</sup>P. Hawrylak, *Phys. Rev. Lett.* **71**, 3347 (1993).